Materials Science and Engineering, 45 (1980) 143 - 152

32

The Effects of Temperature and Pulse Duration on the Shock-loading Response of Nickel

MARC A. MEYERS

Department of Metallurgical and Materials Engineering, New Mexico Institute of Mining and Technology, Socorro, N.M. 87801 (U.S.A.)

H.-J. KESTENBACH

Universidade Federal de São Carlos, São Carlos, SP (Brazil)

CARLOS A. O. SOARES

Center for Materials Research, Instituto Militar de Engenharia, Pca. Gen. Tiburcio-Urca-ZC 82, Rio de Janeiro, RJ (Brazil)

(Received December 21, 1979)

SUMMARY

The effects of driver plate thickness and shock-loading temperature on the shock wave response of nickel were investigated; driver plate thicknesses of 3.18, 6.36 and 25.44 mm and temperatures of 77 and 300 K were used at a constant pressure of 15.7 GPa. Calculations conducted for the three driver plate thicknesses showed that the acceleration histories of the three plates are different; consequently, different stand-off distances were used (5, 10 and 20 mm for the 3.18, 6.36 and 25.44 mm plates respectively). Post-explosion observation by transmission electron microscopy showed that the low temperature events exhibited cell structures that were less well developed than the ambient temperature events. All six events exhibited work softening; the ambient temperature events showed a very slight amount of recovery, as evidenced by the tensile curves. The high pulse duration events (for the 25.44 mm driver plate) exhibited larger cell sizes, at both 77 K and ambient temperature, than did the lower pulse duration events. This is attributed to a substantial deviation from uniaxial strain conditions for the experimental system. It is therefore recommended that further experiments in the high pulse duration range use experimental set-ups where the lateral system dimensions are appropriately scaled up to propitiate a uniaxial strain configuration.

1. INTRODUCTION

As in any deformation process, there are a certain number of parameters that affect the residual mechanical properties and substructure of shock-loaded materials. These can be classified into material parameters (grain size, substructure) and external parameters (temperature, peak pressure, pulse duration, rarefaction rate, planarity of wave, orientation of wave). Of the external parameters, peak pressure was the first parameter to be recognized as important, by Rinehart and Pearson [1], for example. Appleton and Waddington [2] and later Champion and Rohde [3] pointed out the importance of pulse duration. Further investigations [4 - 13] have confirmed the effect of this parameter. While Appleton and Waddington [2], Champion and Rohde [3] and Marsh and Mikkola [11] investigated the effect of pulse durations up to values of around 3 μs, Murr and coworkers [5 - 10] explored the pulse duration range above 0.5 μs (up to 14 μs [7]). In this paper we describe and discuss the results of an investigative effort made in order to attempt to understand the effect of pulse durations better. We realize that the rarefaction rate was

not constant for the three pulse durations used in this investigation. However, it would have been impossible to find a set of three different metals that would provide a constant rarefaction rate for such a wide variation in pulse durations (1.3 - 10.6 μs). The experiments were conducted in such a way that we could determine whether parameters other than pulse duration could possibly be affecting the results. The main effects studied were the substructure recovery at high pulse durations and the driver plate velocity.

1.1. Substructure recovery at high pulse durations

The nominal residual temperatures after the shock waves can be calculated by assuming that the metal has a hydrodynamic response. It is not known, however, to what extent these calculations are accurate. There are, to our knowledge, only three reports of experimental measurements [13 - 15]. Assuming a hydrodynamic response the calculations yield the residual temperature rises as a function of only the peak pressure. For example, the ambient temperature 25 GPa events conducted by Murr and coworkers [5 - 8] are associated with the nominal residual temperatures of [16] 329 K for AISI 304 stainless steel, 419 K for aluminum, 341 K for copper and 348 K for niokel; these temperatures are hardly capable of inducing recovery in these materials. However, since the energy input is higher for large durations, it is possible that higher residual temperatures might be generated, especially if the response of the metal deviates substantially from that predicted by the hydrodynamic hypothesis. Large deviations for the attenuation rates from the rates calculated using the hydrodynamic assumption were in fact found by Rempel *et al.* [17] and by Erkman and Christensen [18].

1.2. Driver plate velocity

No velocity probes or pressure gauges were used in this investigation. Consequently the explosive charges were obtained from calculations involving the Gurney equation [19, 20] and impedance matching, according to Orava and Wittman [21]. However, these calculations only predict a steady state driver plate velocity. They do not account for the fact that the thicker driver plates have a higher inertia and therefore an acceleration history which is different from that of the thinner plates, even if the terminal steady state velocity is the same.

Accordingly, the experiments were designed to test the two effects mentioned above. Firstly, the possible effects of substructure recovery were verified by conducting events under identical pressure and pulse durations but at two widely different temperatures: 77 K and ambient temperature. Any recovery, if present for the ambient temperature events, would certainly be entirely inhibited if the impact were conducted at 77 K. Secondly, driver plate acceleration to its steady state velocity was assumed by allowing increasing driver plate–cover plate separations (stand-off distances) with increasing driver plate thicknesses and associated pulse durations. A calculation procedure for obtaining stand-off distances is presented.

2. EXPERIMENTAL PROCEDURE

Shock loading was accomplished by accelerating explosively driven copper plates onto the samples; a mousetrap-type explosive assembly was used and the samples were protected by a cover plate, lateral momentum traps, and an anvil and spall plate on the lower surface. The details are given elsewhere [22], and only the features not described in ref. 22 are presented here. In each system, five nickel (with an average grain size of 55 μm as determined by the linear intercept method) and two 304 stainless steel strips were positioned side by side, the nickel strips at the center and the stainless steel strips at the edges.

Six different events, all at the same pressure of 15.7 GPa, were conducted. Three events (of pulse durations 1.3, 2.6 and 10.6 μs) were conducted at room temperature and three events at 77 K. Because of the slight differences in shock impedance between nickel and stainless steel, some internal reflections were unavoidable. However, the amplitude of these reflections did not exceed 1.26 GPa (the difference between the pressure generated in nickel and in stainless steel). Table 1 shows the various parameters of the shock-loading events. Both pulse durations and rarefaction rates were calculated (for

TABLE 1

Parameters in shock-loading experiments

Parameter	*Pulse duration*		
	1.3 μs	*2.6 μs*	*10.6 μs*
Pressure, Ni (GPa)	15.7	15.7	15.7
Pressure, 304 stainless steel (GPa)	14.8	14.8	14.8
Terminal driver plate velocity (mm μs^{-1})	728	728	728
Driver plate thickness (mm)	3.18	6.36	25.44
Calculated stand-off distance (mm)	2.2	4.2	17.0
Experimental stand-off distance (mm)	5	10	20
Explosive thickness (mm)	8.8	16.6	70.4
m_e/m_p	0.34	0.34	0.34
Rarefaction rate (GPa μs^{-1})	−51.0	−32.6	−10.3
Temperature (K)	77, 300	77, 300	77, 300
Pulse width (mm)	6.3	2.8	53.3
Transient temperature rise (K) [23]	41	41	41
Residual temperature rise (K) [23]	34	34	34

nickel) using equations given by Orava and Wittman [20]. It can be seen that the rarefaction rate is markedly dependent on pulse duration. It varied from −51.0 GPa μs^{-1} for 1.28 μs to −10.3 GPa μs^{-1} for 10.64 μs. The experimental set-up used for the 77 K events is shown in Fig. 1. A similar technique has been used previously by Rose and Berger [24]. The system and cover plate were inserted in a plastic bag. The plastic bag was filled with nitrogen gas and was flushed three times; the main purpose of the nitrogen atmosphere was to avoid the formation of ice crystals on the driver and cover plate surfaces when they were cooled to liquid nitrogen temperature (77 K). Liquid nitrogen was then introduced into the Styrofoam container and was added until boiling was reduced to a minimum. The explosive charge (line and plane wave generators) was placed on top of the bag; the small layer of plastic was not expected to have an appreciable influence on the driver plate velocity.

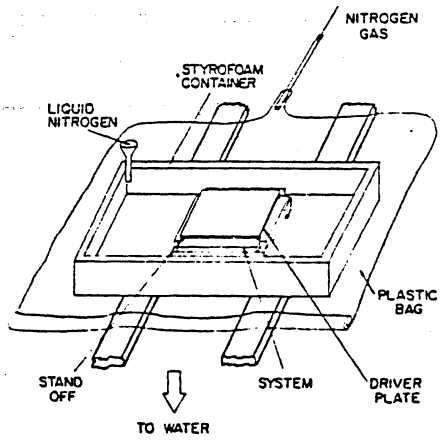

Fig. 1. Experimental set-up used for the 77 K events.

For transmission electron microscopy using a JEOL-100 B electron microscope operated at 100 kV, 3 mm discs were obtained parallel to the surface of the sheets. They were cut from the central portion of the sheets by spark erosion and planing in a Servomet SMD apparatus and were thinned by conventional techniques. The samples were kept at 273 K prior to use to avoid post-explosion recovery.

3. RESULTS

3.1. Stand-off distance

The Gurney equation [19, 20], which is commonly used to obtain the terminal driver plate velocity, has been successfully compared with experimental determinations using switch pins [21]. However, these experiments were conducted for lower driver plate thicknesses (up to 4 mm). One of the deficiencies of the Gurney equation is that it does not take into consideration the acceleration of the driver plate from its initial position. The terminal velocity of the plate is obtained by equating the chemical energy of the explosive to the kinetic energy of the plate. To take into account the drag effect of the air, the usual assumption is that the steady state velocity of the driver plate is equal to 95% of the terminal velocity. The only work, to our

knowledge, that deals with the acceleration of projectiles to their terminal velocity is the paper by Aziz *et al.* [25]. For the conditions used in the present investigation (p = 15.7 GPa in nickel) the Gurney formula predicts the following ratio r of the explosive mass m_e to the plate mass m_p per unit area:

$$r = \frac{m_e}{m_p} = 0.341$$

Since Aziz *et al.* [25] only made computations for values of r between 1 and 10 (higher explosive-to-driver ratios) an extrapolation was required. This was done by a cross-plot using ref. 24, Fig. 4; the result is shown in Fig. 2. The broken portions of the curves are extrapolated values. The ordinates express the ratio of the driver plate velocity U to the terminal driver plate velocity U_t. The various curves apply to different scaled time intervals (Dt/L where D is the detonation velocity, t is the time and L is the explosive charge thickness) after the start of the driver plate motion. For r = 0.341 we obtain the curve shown in Fig. 3 in which the scaled time is plotted against the ratio U/U_t. For the three experiments conducted in the present investigation, r was maintained constant and both the thickness of the driver plate and of the explosive were varied. Figure 4 shows a plot of the driver plate velocity against time. The scaled time and velocity ratios of Fig. 3 were appropriately changed. It is immediately

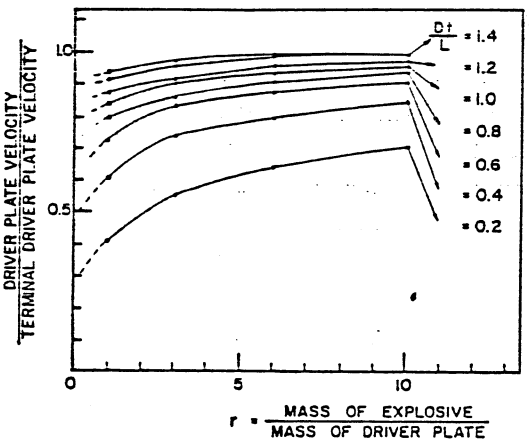

Fig. 2. Plots of the scaled driver plate velocity against the ratio of explosive to the driver plate mass for various values of scaled time Dt/L (where D is the detonation velocity, t is the time and L is the explosive charge thickness) after the start of driver plate motion. (Adapted from Aziz *et al.* [25].)

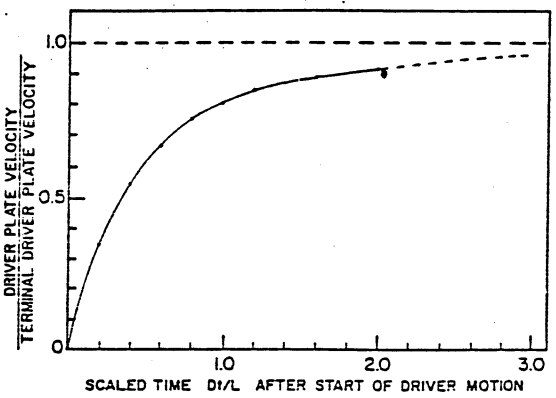

Fig. 3. Plot of the scaled driver plate velocity against the scaled time after the start of driver plate motion for r = 0.341 (this is the ratio for the shock-loading geometry used in the experiments).

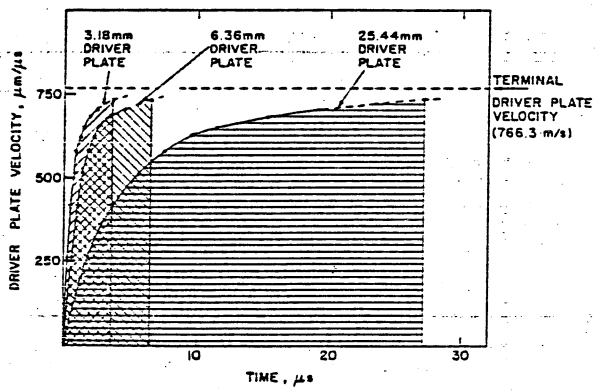

Fig. 4. Plots of the driver plate velocity against time for three different driver plate thicknesses. The areas under the curves provide the required distances.

obvious that, the thicker the explosive and driver plate (at a constant r), the longer it takes for the driver plate to accelerate to its terminal velocity. The fact that the plate is accelerating in air undoubtedly reduces its velocity somewhat. It was therefore assumed that the steady state velocity is equal to 95% of the terminal velocity. Figure 4 shows the times required to reach this steady state velocity (766 m s^{-1}); they are 3.6, 6.6 and 27 μs for the 1.3, 2.6 and 10.6 μs duration events respectively. The areas under these curves provide the distances required for the driver plate to be accelerated to this velocity. The distances required are equal to 2.2, 4.2 and 17.0 mm respectively. These are the calculated stand-off distances. It is not known to what extent these calculations are accurate. However, they show that a proportionality exists between the driver plate thickness (and consequently the pulse duration) and the

stand-off distance. Accordingly the stand-off distances used were 5, 10 and 20 mm for the 1.3, 2.6 and 10.6 μs events respectively.

It should be pointed out that the calculations by Aziz *et al.* [25] were done for $\gamma = 3$ (where γ is the adiabatic expansion coefficient of the gaseous detonation products [18]) whereas the value for Detasheet C, and its Brazilian equivalent Plastex P, should be 2.70 [18]. However, this difference is not expected to have a significant effect on the results.

3.2. Microstructure

The substructures of nickel shock loaded at 300 K (1.3 and 10.6 μs) and 77 K (1.3 and 10.6 μs) are shown in Figs. 5 and 6 respectively. They are composed, for all conditions, mainly of dislocation arrays. Mechanical twinning was very infrequent for the ambient temperature events and somewhat more

(a)

(b)

Fig. 5. Transmission electron micrographs of nickel illustrating typical substructures of 300 K events: (a) 1.3 μs; (b) 10.6 μs.

(a)

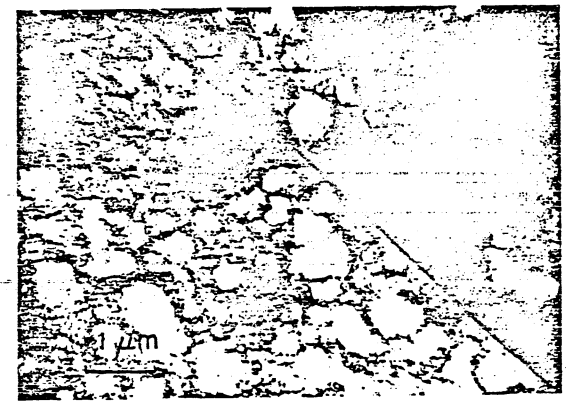

(b)

Fig. 6. Transmission electron micrographs of nickel illustrating typical substructures of 77 K events: (a) 1.3 μs; (b) 10.6 μs.

frequent (although only occasional) for the 77 K events. This was to be expected for the ambient temperature events because the pressure was maintained below the threshold for twinning reported by Nolder and Thomas [26] (35 GPa).

However, there were some noticeable differences in the cell morphology and size. The cell structure of the ambient temperature events was quite well defined, as can be seen from Fig. 5. In contrast, the 77 K events exhibited a more poorly defined cell structure (Fig. 6) and the substructure was rather variable. Figure 6 does not show the rather variable substructure; areas with no defined cell structure coexisted with regions where cell formation could be observed. At 1.3 μs (Fig. 6(a)) a strong alignment of the cell walls along (111) planes was often observed. This alignment was no longer present for the 77 K 10.6 μs event (Fig. 6(b)). The average cell sizes as measured by the linear intercept

method are given in Table 2. The 10.6 μs events show cells between 60% and 90% larger than the 1.3 μs events. For the 77 K event (both 1.3 and 10.6 μs) cell size measurement was somewhat difficult because in many areas there was no clear-cut distinction between the cell interior and the cell walls.

TABLE 2

Cell sizes of shock-loaded nickel

Shock-loading parameter		*Cell size* (μm)
Temperature (K)	*Pulse duration* (μs)	
300	1.3	0.40
300	10.6	0.66
77	1.3	0.36
77	10.6	0.69

3.3. Mechanical behavior

Figure 7 shows the hardness (Rockwell B) of shock-loaded nickel for the three pulse durations. The hardnesses definitely do not show a tendency to drop at the higher pulse duration. If there is any tendency at all, the change is towards a higher hardness. There does not seem to be a significant difference in hardness between the 77 and 300 K events.

The effects of shock-loading pulse duration and temperature on the ambient temperature tensile response of nickel are shown in Fig. 8. These curves present a unique feature in that

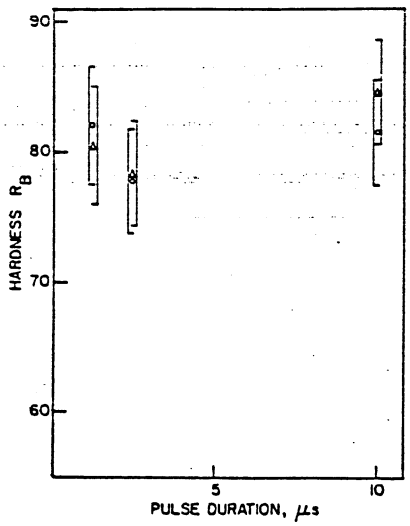

Fig. 7. Hardness of nickel after shock loading for shock-loading temperatures of 77 K (○) and 300 K (△).

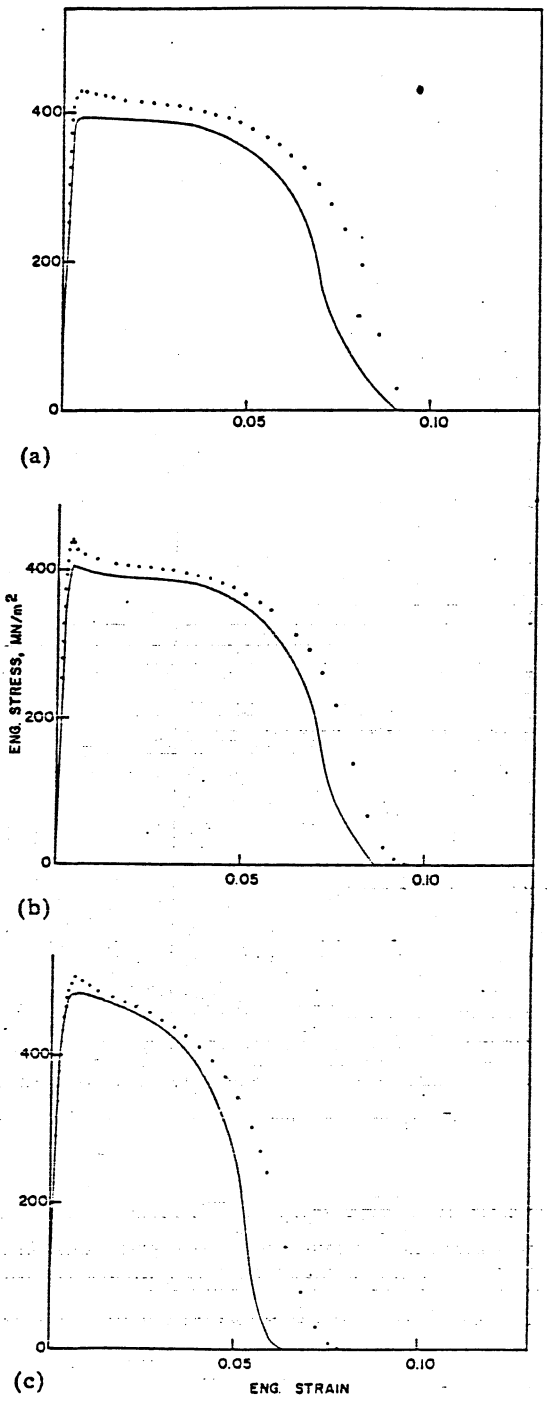

Fig. 8. Plots of ambient temperature engineering stress against engineering strain for (a) 1.3, (b) 2.6 and (c) 10.6 μs events: ——, ambient temperature events; · · ·, 77 K events.

there is nearly coincidence between yield and ultimate stress. This behavior has been ascribed to the inherent instability of the shock-loading substructure under conven-

tionally applied loads; it is known as *work softening* and has been analyzed elsewhere [22]. (The pressure and pulse durations are incorrectly stated in ref. 22. An error was made in the Gurney equation; the real density for Detasheet C-2 was taken as 2 g in^{-2}. Only 71% of the mass is actual explosive, the balance being a binder. Therefore the correct density should be 1.42 g in^{-2}.) The yield and ultimate stresses of the 77 K events seem to be slightly higher than those of the 300 K events, for all durations; the curves have otherwise very similar shapes. The curves for the lower temperature events seem to exhibit more pronounced "ultimate drops" (drops in stress immediately after the ultimate tensile stress is reached). Work softening seems to be slightly more prevalent in the 77 K events. Other specific features brought out by the tensile curves of Fig. 8, and masked by the hardness measurements, are the increases in yield and ultimate tensile stresses with increasing pulse duration, with a concomitant decrease in total elongation.

4. DISCUSSION

We shall first discuss the two effects described in Sections 1.1 and 1.2; then an attempt to rationalize the microstructural and mechanical results will be made.

4.1. Substructure recovery at high pulse durations

Both the cell sizes (the same cell sizes for the same duration, at 77 and 300 K) and the tensile and hardness data rule out the recovery hypothesis. If recovery was substantial, and since it would be inhibited in the 77 K events, these events should exhibit residual properties which are substantially different from those of the 300 K events. The cell sizes of the 10.6 μs events are essentially the same. The hardnesses are very similar. The tensile curves of the 77 K events show a slightly more pronounced *work softening*; however, for the three pulse durations the 77 K events show a consistent difference.

4.2. Driver plate velocity

The calculations based on Aziz *et al.*'s [25] treatment of accelerating projectiles show that the driver plate–system separation is important. If insufficient, the impact velocity, and consequently the pressure, are below the predictions from the Gurney equation and Rankine–Hugoniot calculations. The stand-off distances were accordingly increased for the higher pulse duration experiments; they were 5, 10 and 20 mm for the 1.3, 2.6 and 10.6 μs events respectively. In spite of this, the hardness of the higher pulse duration events was not higher than that for the lower duration events. This is in accord with the recent conclusions reached by Murr and Kuhlmann-Wilsdorf [9].

4.3. Less well-defined cells at 77 K for the 1.3 μs events

The fact that there are less well-defined cells at 77 K for the 1.3 μs events indicates that some rearrangement of the dislocations takes place during the application of the peak pressure pulse, and this rearrangement is inhibited for the 77 K event. Murr and Kuhlmann-Wilsdorf [9] recently found that the cells become more well defined with increasing pulse duration. For the 77 K events the transient temperature is still very low (see Table 1) and it is thought that thermal activation is not sufficient for substantial rearrangement. Therefore the substructure is probably very close to the substructure originally generated.

The tensile results depicted in Fig. 8 agree with the substructural observations. The 77 K events show consistently a more pronounced *work softening* than the ambient temperature events do. This would be the case if the 77 K samples had a more uniformly distributed dislocation substructure, because more dislocation motion would be required before the substructure was transformed into the substructure stable for conventional deformation conditions at ambient temperature.

4.4. Larger cells for the 10.6 μs events at both 77 and 300 K

Murr and Kuhlmann-Wilsdorf's [9] observations on residual substructures of shock-loaded nickel predict a dislocation density and cell size independent of the pulse duration. However, this was not the case in the present investigation, as can be seen in Figs. 5 and 6 and in Table 2. The reason for the larger cells for the 10.6 μs duration events is thought to be connected with the geometry

TABLE 3

Reduction in thickness of nickel and AISI 304 stainless steel

Pulse duration (μs)	*Temperature* (K)	*Reduction in thickness (%)*		*Sample width/pulse width* (mm mm^{-1})
		Ni	*304 stainless steel*	
1.28	77	0.5	0	101.6/6.3
1.28	300	0.9	0	101.6/6.3
2.61	77	2.3	1.4	101.6/12.8
2.61	300	2.3	0	101.6/12.8
10.64	77	12.9	4.6	101.6/53.3
10.64	300	20.7	5.5	101.6/53.3

of the shock-loading assembly, as will become clear from the discussion that follows. Table 3 shows the reductions in thickness undergone by nickel and AISI 304 stainless steel samples due to the passage of shock waves. These reductions are higher for the ambient temperature events and higher durations. The results in Table 3 show that at higher pulse durations the conditions of uniaxial strain required for shock waves were relaxed; this is especially the case for the 10.6 μs ambient temperature event for nickel. The reduction in thickness was 20.7%. It is instructive to calculate the transient strain introduced by the shock wave and to compare it with the residual strain. The effective strain is the best measure of overall deformation undergone by a material. From the Hugoniot curve for nickel we obtain the ratio of the compressed specific volume to the initial specific volume: $V/V_0 = 0.934$ [27]. The effective strain ϵ^* is defined [28] by

$$\epsilon^* = \frac{2^{1/2}}{3}\{(\epsilon_1 - \epsilon_2)^2 + (\epsilon_2 - \epsilon_3)^2 + (\epsilon_3 - \epsilon_1)^2\}^{1/2}$$

Since $\epsilon_2 = \epsilon_3 = 0$, the effective strain ϵ_f^* at the front is given by

$$\epsilon_f^* = \tfrac{2}{3}|\epsilon_1| = \tfrac{2}{3}\left|\ln\left(\frac{V}{V_0}\right)\right| = 0.046$$

The total strain generated by shock loading is under ideal conditions the sum of the strains introduced at the shock front and at the rarefaction portion of the wave. Assuming them to be equal, we have a total strain of

$$\epsilon_s^* = 2\epsilon_f^* = 0.091$$

The effective strain ϵ_r^* corresponding to the residual deformation found in the sample is given by the same expression. Since the volume remained constant and assuming that the lateral strains ϵ_2 and ϵ_3 are equal, we have

$$2\epsilon_2 + \epsilon_1 = 0$$

$$\epsilon_2 = \epsilon_3 = -\frac{\epsilon_1}{2} = -\frac{\ln(-0.207 + 1)}{2} = -0.116$$

and

$$\epsilon_r^* = 0.1728$$

The residual effective strain ϵ_r^* is higher than the transient shock effective strain ϵ_s^*. Residual strains are typically generated by stress waves that operate under a state of uniaxial stress. The state of strain introduced by shock loading produced by normal waves is, by its very nature, a state of uniaxial strain. Certain geometric criteria have to be satisfied for its accomplishment: no lateral flow of matter can take place. The important ratio is the ratio of the pulse width to the lateral dimensions of the specimens. If the lateral dimensions of the specimen are small with respect to the pulse width, the state will be one of uniaxial stress. This state is obtained in Hopkinson bars [29]. A truly uniaxial strain state will result in no dimensional change; deviation from this state will induce progressive changes in the residual dimensions. This was observed in the shock-loaded samples and is shown in Table 3. The reductions in thickness of the samples were measured. It can clearly be seen that, as the pulse duration increases, so does the reduction in thickness. For nickel this reduction increased from zero to around 20%. For AISI 304 stainless steel (which has a higher initial strength) it went from zero to a maximum of 5.5%. Similar results have been reported by Mantaroshin *et al.* [4]. This shows that the experimental assembly used is not appropriate for higher pulse durations. The ratios of the sample width (101.6 mm) to the pulse width

are shown in Table 3. For the 10.6 μs duration this ratio is approximately 2. The reductions in thickness indicate that it is excessive. Therefore superimposed on the uniaxial strain imparted by shock loading (at both the shock and the rarefaction part of the wave) there is a uniaxial stress component resulting in plastic deformation (reduction in thickness). When the medium is bound, as in the Hopkinson bar [28], impacts generate a uniaxial stress configuration. It can therefore be concluded that the deformation undergone by the 10.6 μs nickel samples is intermediate between uniaxial stress and uniaxial strain. Hence we cannot speak in a strict sense of shock waves. Rather, we must use the term "plastic waves" [28]. There have been very few attempts to correlate the two [29]. For the case under discussion (nickel at 10.6 μs) we probably have a hybrid situation.

5. CONCLUSIONS

(a) Calculations were performed which show that the driver plate–system separation prior to shock loading has to be adjusted to allow the driver plate to accelerate to its steady state velocity. The separation should increase with driver plate thickness.

(b) It is shown that the extent of recovery undergone by shock loading nickel at a pressure of 15.7 GPa and with pulse durations of 1.3, 2.6 and 10.6 μs is small. This was established by conducting experiments at ambient temperature and 77 K and obtaining similar hardnesses, ambient temperature tensile curves and cell sizes. The limited recovery can be seen by the slightly more pronounced *work softening* exhibited by the samples shock loaded at 77 K and by the less distinct cell formation for these samples.

(c) The dislocation substructure exhibited by the samples shock loaded at 77 K and 1.3 μs is characterized by a uniform distribution of dislocations aligned in {111} planes. Cell formation is incipient. This dislocation substructure should be the one that most resembles the substructure originally generated by shock loading.

(d) The appreciable residual deformations undergone by nickel at the 10.6 μs duration events (a reduction in thickness of 12.9% for the 77 K event and a reduction in thickness of 20.7% for the ambient temperature event) suggest that the plastic wave traversing the metal deviates considerably from an ideal shock wave. It is suggested that this deviation which transforms the shock wave into a plastic wave is responsible for the larger cell sizes at the high pulse duration events. The only solution to this problem is a scale-up of the system in order to maintain the uniaxial strain state.

ACKNOWLEDGMENTS

This work was supported by the Brazilian Army and FINEP through the Materials Research Center, Instituto Militar de Engenharia. Ashok Dhere and Marambaia Proving Grounds personnel were extremely helpful in the execution of the explosions. The many fruitful discussions with Professors J. R. C. Guimarães and R. N. Orava were very important in the development of the experimental program described in this paper. A National Science Foundation Grant DMR-7927102 is gratefully acknowledged by one of us (M. A. M.).

REFERENCES

1 J. S. Rinehart and J. Pearson, *Behavior of Metals under Impulsive Loads*, American Society for Metals, Metals Park, Ohio, 1954; Dover Publications, New York, 1964, p. 184.
2 A. S. Appleton and J. S. Waddington, *Acta Metall., 12* (1964) 956.
3 A. R. Champion and R. W. Rohde, *J. Appl. Phys., 41* (1970) 2213.
4 A. P. Mantaroshin, G. M. Nagornov and P. O. Pashkov, *Phys. Met. Metallogr. (U.S.S.R.), 29* (1970) 145.
5 L. E. Murr and M. L. Sattler, *Scr. Metall., 8* (1974) 1477.
6 L. E. Murr and K. P. Staudhammer, *Mater. Sci. Eng., 20* (1975) 35.
7 K. P. Staudhammer and L. E. Murr, *Proc. 5th Int. Conf. on High Energy Rate Fabrication, Denver Research Institute, University of Denver, Colorado, June 1975*, p. 1.7.1.
8 L. E. Murr and J.-Y. Huang, *Mater. Sci. Eng., 19* (1975) 115.
9 L. E. Murr and D. Kuhlmann-Wilsdorf, *Acta Metall., 26* (1978) 847.
10 E. Moin and L. E. Murr, *Scr. Metall., 12* (1978) 575.
11 E. T. Marsh and D. E. Mikkola, *Scr. Metall., 10* (1976) 851.
12 S. LaRouche and D. E. Mikkola, *Scr. Metall., 12*

(1978) 543.
13 J. W. Taylor, *J. Appl. Phys., 34* (1963) 2727.
14 R. G. McQueen, E. Zukas and S. March, *Symp. on Dynamic Behavior of Metals, University of New Mexico, Albuquerque, New Mexico, 1962*, p. 306.
15 W. G. Von Holle and J. J. Trimble, *J. Appl. Phys., 47* (1976) 2391.
16 R. Kinslow (ed.), *High-velocity Impact Phenomena*, Academic Press, New York, 1970, Appendixes A and D.
17 J. R. Rempel, D. N. Schmidt, J. O. Erkman and W. M. Isbell, *Tech. Rep. WI-TR-64-119*, 1966, Stanford Research Institute (Air Force Weapons Laboratory AD62796, Contract AF-29(601)-6040).
18 J. O. Erkman and A. B. Christensen, *J. Appl. Phys., 38* (1967) 5395.
19 R. W. Gurney, The initial velocities of fragments from bombs, shells, and grenades, *Rep. 405*, September 14, 1943, Ballistic Research Laboratories, Aberdeen Proving Ground, Ministry of Defence.
20 J. E. Kennedy, in L. Davidson *et al.* (eds.), *Proc. Conf. on Behavior and Utilization of Explosives in Engineering Design, Albuquerque, New Mexico, 1972*, pp. 125 - 148.
21 R. N. Orava and R. H. Wittman, *Proc. 5th Int. Conf. on High Energy Rate Fabrication, Denver Research Institute, University of Denver, Colorado, June 1975*, p. 1.1.1.
22 M. A. Meyers, *Metall. Trans. A, 8* (1977) 1581.
23 M. H. Rice, R. G. McQueen and J. M. Walsh, *Solid State Phys., 6* (1958) 1.
24 M. F. Rose and T. L. Berger, *Philos. Mag., 17* (1968) 1121.
25 A. K. Aziz, H. Hurwitz and H. M. Sternberg, *Phys. Fluids, 4* (1961) 380.
26 R. L. Nolder and G. Thomas, *Acta Metall., 12* (1964) 227.
27 R. G. McQueen and S. P. Marsh, *J. Appl. Phys., 31* (1960) 7253.
28 J. D. Lubahn and R. F. Felgar, *Plasticity and Creep of Metals*, Wiley, New York, 1961, p. 286.
29 R. J. Wasley, *Stress Wave Propagation in Solids: An Introduction*, Dekker, New York, 1973, p. 206.
30 R. J. Wasley and F. E. Walker, *J. Appl. Phys., 40* (1969) 2639.